Difference FTIR Studies Reveal Nitrogen-Containing Amino Acid Side Chains Are Involved in the Allosteric Regulation of RecA†

Catherine M. Schwartz, Penny M. Drown, and Gina MacDonald*

Department of Chemistry, James Madison University, Harrisonburg, Virginia 22807

Received December 16, 2004; Revised Manuscript Received April 5, 2005

ABSTRACT: The *Escherichia coli* RecA protein performs the DNA strand-exchange reaction utilized in both genetic recombination and DNA repair. The binding of nucleotides triggers conformational changes throughout the protein resulting in the RecA−ATP (high DNA affinity) and RecA−ADP (low DNA affinity) structures. Difference infrared spectroscopy has allowed us to study protein structural changes in RecA that occur after binding ADP or ATP. Experiments were performed on control and uniformly ^{15}N-labeled RecA in an effort to assign vibrational changes to protein structures and study the molecular changes associated with the allosteric regulation of RecA. Comparison of RecA−ATP and RecA−ADP data indicates that the protein adopts unique secondary structures in each form and altered N−H stretching vibrations in the RecA−ADP structure not observed in the RecA−ATP data. Numerous vibrations throughout the 1700−1300 cm^{-1} region are influenced by isotopic substitution and imply that many nitrogen-containing side chains are altered after ADP binds to RecA. The RecA−ATP data contain unique vibrations that are not observed in the RecA−ADP data and may be associated with Gln, Lys, Arg, or Asn. Model compound studies on control and ^{15}N-labeled glutamine and lysine provide additional evidence that supports the tentative assignments of vibrations observed in our difference spectra. In addition, we provide evidence that nitrogen-containing amino acids are important in locking in the low-DNA affinity, more compact conformation of the protein and that some of these interactions may not be present in a more extended, flexible RecA−ATP conformation.

The *Escherichia coli* RecA protein performs the DNA strand-exchange reaction utilized in both genetic recombination and DNA repair. RecA is also responsible for the initiation of the SOS response and the repair of stalled replication forks (*1*, *2*). RecA homologues have been found in all major kingdoms of living organisms (*3*, *4*). The nucleotide-binding site for ATP and ADP is the most highly conserved region in the RecA protein and contains sequences that match the Walker A and B boxes (*4*, *5*). Binding of nucleotide to the site results in the transmission of information throughout the protein, modulates monomer−monomer interactions, and results in the allosteric regulation of RecA. ATP binding yields a protein filament with a high affinity for DNA, while ADP binding induces a lower-affinity protein filament (*6*). RecA-catalyzed ATP hydrolysis is normally dependent on ssDNA[1] but can be initiated by the presence of high salt (*7*). Small-angle neutron scattering studies have shown that the RecA filament is elongated upon binding nucleotide and that this extension is further enhanced in the presence of high salt (*8*). Recent fluorescence experiments have shown that the inactive RecA filament cannot directly be converted to an active filament when ATPγS binds but must disassemble first before forming an active structure (*9*). Thus, it is clear that interactions between monomers are crucial to the allosteric regulation of RecA.

Monomer−monomer interactions result in a variety of filamentous structures whose forms are dictated by solution conditions as well as by DNA and nucleotide binding. Electron microscopy has been used extensively to study the wide range of filamentous structures of RecA (*10*, *11*). The many forms of the inactive filament include RecA, RecA−DNA, and RecA−DNA−ADP filaments (reviewed in refs *10* and *12*). These inactive forms of the protein filament are more compressed than the active nucleoprotein filament (RecA−ssDNA−ATP) that exists in an extended helical conformation that is required for both DNA strand exchange and LexA cleavage (*4*, *10*, *12*). Recent EM experiments with RecA−DNA filaments have shown that nucleotide binding results in the rotation of the C-terminal lobe of the RecA protein and ATP binding between subunits (*13*). This may help explain the cooperativity between RecA monomers. Furthermore, the EM reconstructions indicate that Phe217 is inserted farther into the neighboring subunit when ATP is bound (*13*). In addition, studies of the RecA−ATP filaments reveal that Lys248, Lys250, and Pro254 are near the adenosine base of the ATP associated with the neighboring subunit (*13*). Studies on C-terminal mutations also reveal

† This research was supported by National Science Foundation Grant MCB-9733566 and NSF-REU Grant CHE-0097448.

* To whom correspondence should be addressed: Department of Chemistry, James Madison University, Harrisonburg, VA 22807. Phone: (540) 568-6852. Fax: (540) 568-7938. E-mail: macdongx@jmu.edu.

[1] Abbreviations: FTIR, Fourier transform infrared spectroscopy; HEPES, 4-(2-hydroxyethyl)piperazine-1-ethanesulfonic acid; Tris, tris-(hydroxymethyl)aminoethane; caged ATP or NPE-ATP, P^3-[1-(2-nitrophenyl)ethyl]adenosine 5′-triphosphate; caged ADP or NPE-ADP, P^3-[1-(2-nitrophenyl)ethyl]adenosine 5′-diphosphate; ATPγS, adenosine 5′-*O*-(thiotriphosphate); ssDNA, single-stranded DNA; dsDNA, double-stranded DNA.

10.1021/bi047362u CCC: $30.25 © 2005 American Chemical Society
Published on Web 06/23/2005

that this region of the protein may be involved in important interactions between monomers that help to modulate the activity of RecA (*14*−*16*).

Three-dimensional crystal structures of RecA obtained in the absence of nucleotide or the presence of ADP show that both of the resulting protein filaments have a pitch of ∼83 Å (*17*, *18*). RecA contains N-terminal and C-terminal domains and a core domain that contains the nucleotide-binding site (*17*, *18*). Story and Steitz (*17*, *18*) identified two disordered loops, L1 and L2, that were proposed to be involved in DNA binding. More recent studies of RecA filaments with pitches of ∼74 Å show that when compared to the ∼83 Å structure the compressed structures have the largest differences in the orientation of the C-terminal domain and only six of 25 contacts that occur at the monomer−monomer interface move more than 1 Å (*19*). The most interesting movements at the subunit interface involve lysines 6 and 250 along with changes in Arg28 and Arg222 (*19*). New structures have also been obtained on RecA complexed with MgADP and MnAMP-PNP. They show a few differences in the P-loop residues; however, it was found that neither cofactor can activate RecA, and the authors speculated that the RecA−MnAMP-PNP structure represents a "preisomerization" state of the RecA−ATP complex (*20*). Structures of the RecA protein from *Mycobacterium tuberculosis* ($RecA_{Mt}$) and *Mycobacterium smegmatis* ($RecA_{Ms}$) complexed with NTP analogues have also been obtained (*21*, *22*). The $RecA_{Mt}$ and $RecA_{Ms}$ structures reveal that the geometry of the nucleotide-binding site itself is rather rigid, yet the positions of the nucleotides vary between complexes (*21*, 22). The pitch of the filaments in the recent structures resembles that of the more compressed *E. coli* RecA filaments and suggests that important residues around the nucleotide-binding site include Asn, Arg, Asp, Lys, Thr, Tyr, and Gln (*20*−*22*).

Saturation mutagenesis studies that suggest key roles for Gln194, Lys198, and Arg196, combined with spectroscopic studies of L2, have led to an active site model that resembles the NTP pockets of G-proteins (*23*, *24*). Additional studies have determined that Lys72 is crucial for ATP hydrolysis, Asp100 is involved in nucleotide specificity, and Gln194 plays a crucial role in the allosteric switching mechanism (*25*−*27*). Many RecA studies have focused on the characterization of numerous mutants that are extensively reviewed by McGrew and Knight (*12*). Although it is clear that the nature of the bound nucleotide regulates specific contacts between neighboring monomers, there are various theories about the amino acids involved in the transfer of information from the cofactor-binding site to the oligomeric interface (*4*, *12*, *13*). The crystal structures that have been obtained have provided incredible insights into important structural modifications; however, molecular-level information about the more extended helical conformation of RecA that is associated with ATP hydrolysis remains somewhat elusive. Additional techniques are necessary to more accurately define the protein changes associated with the allosteric regulation of RecA and to ultimately study how RecA structural changes are coupled to ATP hydrolysis. Numerous structural insights have been gained through the use of ATP analogues in conjunction with EM and crystal studies as described above. However, there are likely to be some structural differences between the RecA−analogue and RecA−ATP structures. Difference infrared spectroscopy has provided information about the RecA−ATP conformation that is not easily obtained using other spectroscopic techniques (*28*, *29*). The ability to use an external, photolytic trigger to release ATP from its caged complex and initiate binding to RecA in the infrared cell has allowed us to observe vibrational changes associated with binding of ATP to RecA (*28*, *29*). Studies of RecA in the high-salt or aggregated conformations have hindered the use of other techniques that can provide molecular-level information about conformational changes induced by nucleotide binding. However, difference infrared spectroscopy is especially useful in the study of proteins such as membrane proteins, or aggregated proteins, that are incompatible with other spectroscopic techniques (*30*, *31*). In addition to the high-resolution (0.2 Å) structural information that can be obtained, infrared spectroscopy also allows the observation of protein structural changes that occur over time (*30*).

Difference FTIR experiments have identified key structures that mediate nucleotide-induced changes and have helped to elucidate the molecular mechanisms of numerous proteins (*30*, *32*, *33*). Previous studies in our laboratory have focused on utilizing difference infrared spectroscopy to identify protein structural variations between the ADP- and ATP-bound forms of RecA in the absence of DNA. Difference infrared data obtained by subtracting the RecA spectrum from that of the RecA−ATP or RecA−ADP complex imply that unique secondary structures and amino acid side chain conformations are associated with each of the two RecA conformations (low and high DNA affinity) (*28*, *29*). Our previous results support mutagenesis studies and provide spectroscopic evidence that residues such as Gln, Arg, Lys, Glu, Asp, and Tyr may be critical in controlling the allosteric regulation of RecA (*28*, *29*). These experiments utilized caged ATP and low temperatures and thus allowed the study of the RecA−ATP structure. The infrared studies of the RecA−ATP complex provide additional information that is complementary to studies performed on RecA−analogue complexes. However, infrared difference spectra contain information about both protein vibrations that are affected by nucleotide binding and nucleotide vibrations that are perturbed upon binding. Unfortunately, protein and nucleotide vibrations are located in the same complex region of the spectrum (1800−900 cm^{-1}) (*34*−*37*). To further identify the origins of the vibrations present in our initial data, we have utilized global ^{15}N labeling of RecA in conjunction with difference FTIR. In a previous study, we found that we were able to follow slow structural changes and residual nucleotide binding that occur after the initial photolysis reaction. The new data acquisition procedure that follows changes over time also seems to better identify contributions from single amino acid side chains and decrease the broad contributions, possibly from filament reorganization or nucleotide changes that occur upon initial binding (*29*). The data presented here show that numerous protein vibrations are affected by isotopic substitution and substantiate the fact that Arg, Lys, Gln, and Asn most likely are key residues involved in the allosteric regulation or RecA. Model compound studies on control and ^{15}N-labeled glutamine and lysine provide additional evidence that supports the assignments of vibrations observed in our difference spectra. In addition, we provide evidence that nitrogen-containing amino acids are important

in locking in the low-DNA affinity, more compact conformation of the protein and that some of these interactions may not be present in a more flexible RecA−ATP conformation.

MATERIALS AND METHODS

Protein Expression and Purification. RecA was overexpressed in *E. coli* strain STL327 cells that were transformed with pAIR79 and pT7POL26 [Belgian Co-ordinated Collections of Micro-organisms (BCCM)] plasmids and grown in control or [^{15}N]Celtone (Martek Biosciences Corp.) medium with appropriate antibiotics. The STL327 strain and pAIR79 plasmid were the generous gift of M. Cox. Expression was induced with 1 mM IPTG at an OD_{600} of 0.5 and then grown for approximately 3−4 h at 37 °C following induction. The protein was purified according to the procedure described by Cox with minor modifications (*38*). The protein was eluted from the final ssDNA column with 50−160 mM NaCl instead of using ATP to elute the protein. Fractions containing a single band on SDS−PAGE gels were pooled and precipitated with ammonium sulfate. Finally, the protein pellet was resuspended and dialyzed overnight against buffer M that contained 1 mM $MgCl_2$, 1 mM DTT, 0.1 mM EDTA, and 20 mM Hepes (pH 7.5) and then frozen. ATP hydrolysis was monitored in buffer M (with ssDNA) or a buffer that contained 100 times (100× buffer M) greater concentrations of the components in buffer M (no DNA) to determine rates of hydrolysis under conditions more similar to those in the IR cell (*29*).

Difference Infrared Experiments. Each sample contained approximately 10 nmol of RecA and 200−270 nmol of caged nucleotide. The caged nucleotides, NPE-ATP {P^3-[1-(2-nitrophenyl)ethyl]adenosine 5′-triphosphate (or diphosphate, caged-ADP)}, were purchased from Molecular Probes (Eugene, OR). The protein and caged nucleotides were prepared in buffer M. In addition, approximately 5 mol of dithiothreitol was added for every mole of caged nucleotide to scavenge the cage after photolytic release. Samples used for difference infrared experiments were slowly, partially dehydrated by passing a stream of nitrogen over the samples (on ice) as described previously (*29*). Protein samples were partially dehydrated to decrease the strong water absorption that can interfere with the generation of high signal-to-noise difference infrared data. This dehydration results in a thin film of protein on the infrared window. We estimate that approximately 1 μL of water is present in our protein films, resulting in a final concentration of approximately 10 mM RecA and 200−270 mM caged nucleotide. The dehydration is necessary to decrease the strong water absorption in the amide I region. Infrared spectra were obtained as previously described with the exception that the samples were cooled to 0 to −3 °C (*29*). Infrared spectra were recorded before photolysis, and two spectra were ratioed to ensure no changes were observed before the photolytic release of the cage (*29*). Infrared absorbance spectra were obtained by ratioing spectra taken before photolysis against a spectrum of the calcium fluoride windows to generate the spectra shown in Figure 1. Photolysis was initiated using a nitrogen laser (337 nm). The time-dependent data were obtained by recording a spectrum immediately after the release of caged nucleotide (0 min) and every 10 min thereafter for a total of 70 min (Figure 2). The time-dependent difference data were obtained by ratioing spectra taken 10 or 40 min after release against the spectrum obtained immediately after the release (see Figure 2). Three difference spectra obtained on three separate protein samples were then averaged. The amide I intensity obtained from averaged protein absorbances was then used to normalize the protein content between samples for comparison (Figures 3, 4, 8, and 10) and to generate the double-difference data (Figures 5 and 9).

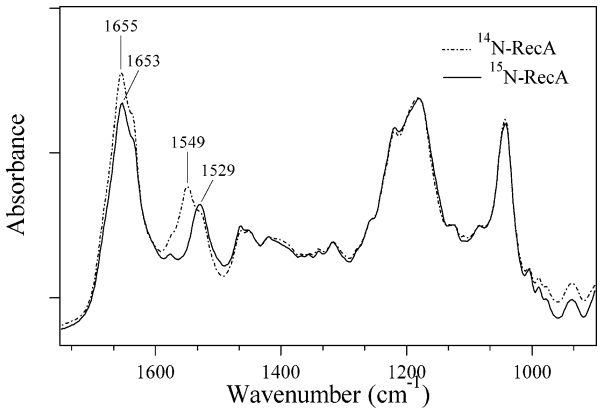

FIGURE 1: Absorbance spectra of control [^{14}N]RecA and caged ADP (dashed line) and uniformly labeled [^{15}N]RecA and caged ADP (solid line) samples. Each spectrum is an average of three samples. The tick marks on the *y* axis correspond to 0.3 absorbance unit.

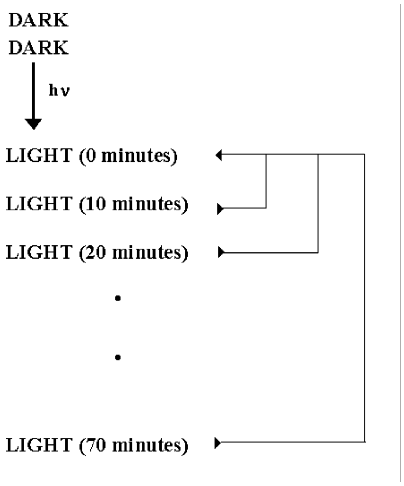

FIGURE 2: Data acquisition scheme used to generate the difference spectra presented in Figures 3, 4, 8, and 10. A spectrum is taken immediately following photolysis (0 min), and then subsequent spectra are taken every 10 min. The spectra taken at 10 min intervals are ratioed to the spectrum taken immediately after photolysis to isolate changes that occur after the photolytic release of the cage.

Infrared Absorbance Spectra of Amino Acids. Infrared spectra of amino acids were obtained on 20 mg/mL solutions of L-Glutamine (Sigma catalog no. G-7029), L-lysine dihydrochloride (Sigma catalog no. L-5751), [*amide*-^{15}N]-L-glutamine (Cambridge catalog no. NLM-557), and [ϵ-^{15}N]-L-lysine-2HCl (Cambridge catalog no. NLM-631) in buffer M. Infrared spectra were recorded using a Nicolet 560 Magna spectrometer that was equipped with a MCT/A detector and a Smart goldengate ATR accessory (Specac). The resolution of the spectra was 4 cm^{-1}. Five hundred scans were co-added for each interferogram with the use of a mirror velocity of 1.8988 cm/s and a Happ−Genzel apodization function. Amino acid spectra were ratioed against absorbance spectra

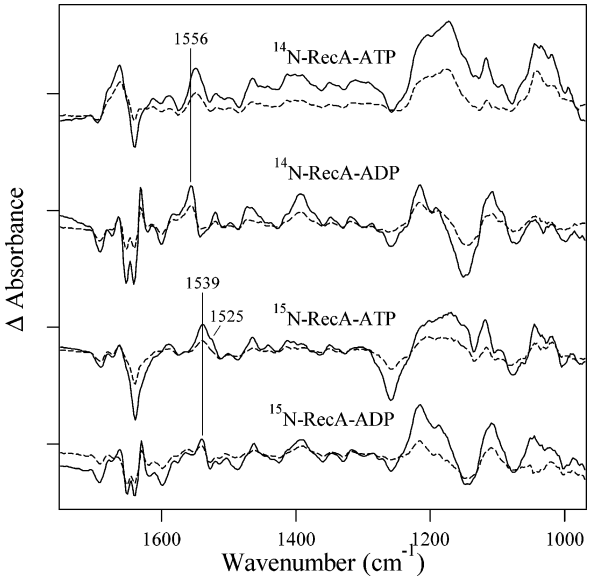

FIGURE 3: Difference infrared spectra generated using the method described in the legend of Figure 2. Data taken at 10 min (dashed lines) and 40 min (solid lines) were ratioed to the spectra taken immediately after photolysis. Difference spectra were obtained for samples that contained caged nucleotides (ATP or ADP) and either control, [^{14}N]RecA, or ^{15}N-labeled RecA. Each spectrum is an average of three spectra obtained on three different samples. To compare intensities of the various spectra, the amide I vibration of averaged absorbance spectra was used to normalize for protein content. The tick marks on the *y* axis correspond to 2×10^{-3} absorbance unit.

of buffer M, and two absorbance spectra were then averaged to obtain the spectra shown in Figures 6 and 7. The ^{15}N absorbance spectrum was subtracted from the ^{14}N absorbance spectrum of the corresponding amino acid to generate the insets shown in Figures 6 and 7.

RESULTS

Characterization of Isotopically Labeled RecA. [^{14}N]RecA control and isotopically ^{15}N-labeled samples were grown and purified under identical conditions and yielded similar rates of ATP hydrolysis. ATP hydrolysis occurred with turnover numbers ranging from 15 to 20 min^{-1} for RecA preparations assayed in the absence of glycerol (buffer M) at 37 °C. Hydrolysis assays with RecA in 100× buffer M [100 mM $MgCl_2$, 100 mM DTT, 10 mM EDTA, and 2 M Hepes (pH 7.5)], in the absence of DNA, were performed to mimic the high buffer salt concentrations present in the infrared samples after dehydration and yielded ~20% of the activity observed in the presence of DNA. Previous studies in our laboratory have shown that RecA that has been dehydrated and rehydrated retains the ability to hydrolyze ATP and have also confirmed that the caged nucleotides used for these studies do not inhibit ATP hydrolysis or interfere with the formation of an active RecA−ATPγS−DNA filament (*28*, *29*).

Figure 1 shows the infrared absorption spectra of control and ^{15}N samples of RecA and caged ADP samples. Similar results were obtained with RecA and caged ATP samples (data not shown). Comparison of the control and globally ^{15}N-labeled RecA absorbance spectra in Figure 1 reveals shifts of the amide I and amide II absorptions that arise from the peptide backbone and are sensitive to hydrogen bonding and the secondary structural composition of the protein (*34*). The amide I vibration is predominately due to the C═O stretching vibration with small contributions from the C−N stretch of the peptide backbone (*34*). Figure 1 shows that incorporation of ^{15}N results in shifts from 1655 to 1653 cm^{-1}, and the shoulder at 1635 cm^{-1} shifts to around 1633 cm^{-1} after isotopic incorporation. The amide II absorption arises from the C−N stretching and N−H bending vibrations of the peptide backbone (*34*) and shifts from 1549 to 1529 cm^{-1} after ^{15}N labeling. The lack of the original 1549 cm^{-1} vibration in the [^{15}N]RecA absorbance spectrum suggests that nearly complete ^{15}N labeling of the protein was achieved.

Time-Dependent Changes Due to Binding of Nucleotide to RecA. Figure 2 shows the data acquisition scheme used for the difference infrared experiments. Two spectra are recorded before photolysis of the caged nucleotide. These spectra are designated DARK in Figure 2. When the two dark spectra are ratioed, no significant changes are observed, and we achieve a signal-to-noise ratio similar to that previously observed (*29*). The photolysis reaction results in the release of the nucleotide from its caged complex and subsequent nucleotide binding to RecA. The first light spectrum taken after photolysis will contain contributions from nucleotide binding and vibrations associated with the release of the nucleotide from its caged complex. The subsequent LIGHT spectra taken every 10 min after photolysis contain contributions that change over time after the release of the nucleotide. Difference spectra presented in this paper were obtained by ratioing subsequent light spectra to the first spectrum taken after photolysis. This method allows us to isolate vibrations associated with the slow structural changes or continued nucleotide binding that occurs over time in the absence of any subtraction artifacts, broad changes that arise from the initial reorganization of the RecA filament, or nucleotide changes that may overshadow smaller changes associated with specific side chain interactions and isotopic shifts (*28*, *29*). In the data presented in Figure 3, we are not able to differentiate between additional nucleotide binding and slow structural changes. Furthermore, any interactions of the cage with the protein or cage with nucleotide may contribute to the spectra. However, cage or nucleotide vibrations are not affected by isotopic labeling of the protein.

Each spectrum presented in Figure 3 is an average of three spectra obtained on three different infrared samples. Each average was normalized using the amide I (~1650 cm^{-1}) absorbance for comparison. It is interesting to note that the later data (40 min) are nearly identical to the initial data (10 min) with the exception of the increased intensities of the vibrations. The data presented in Figure 3 indicate that changes occur for the duration of the experiment. For this reason, we chose to use data obtained when the changes are near completion (40 min) for further analysis. Spectra of the caged nucleotides alone show some small, variable changes with time (data not shown) unlike the reproducible infrared spectra associated with RecA−nucleotide complexes. In this paper, we will focus on only those vibrations that shift upon isotopic incorporation and can be unambiguously identified as protein vibrations. Upon initial inspection of the data presented in Figure 3, we observe clear shifts that arise from nitrogen-containing protein residues. Of particular interest are the amide II vibrations arising from the C−N and N−H vibrations of the peptide backbone. In control [^{14}N]RecA−

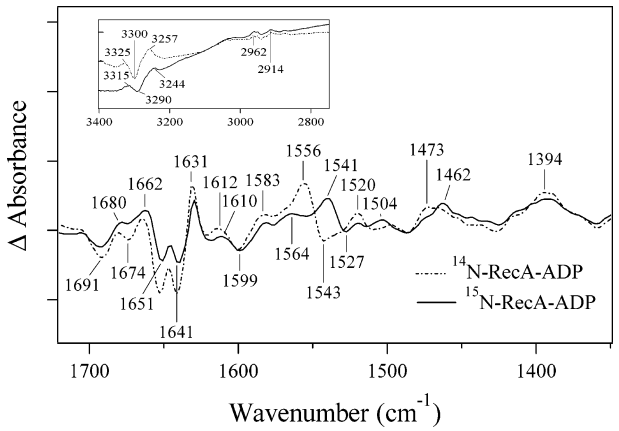

FIGURE 4: Difference spectra obtained by ratioing the spectrum taken at 40 min to the spectrum taken immediately after photolysis. RecA−ADP minus RecA difference spectra obtained for samples that contained caged ADP and either control, [^{14}N]RecA (dashed line), or ^{15}N-labeled RecA (solid line). Each spectrum is an average of three spectra obtained on three different samples. To compare intensities of the various spectra, the amide I vibration of averaged absorbance spectra was used to normalize for protein content. The tick marks on the *y* axis correspond to 1×10^{-3} absorbance unit. The inset shows the 3000 cm^{-1} region of the same spectra: [^{14}N]RecA (dashed line) and ^{15}N-labeled RecA (solid line). The tick marks on the *y* axis of the inset correspond to 1×10^{-3} absorbance unit.

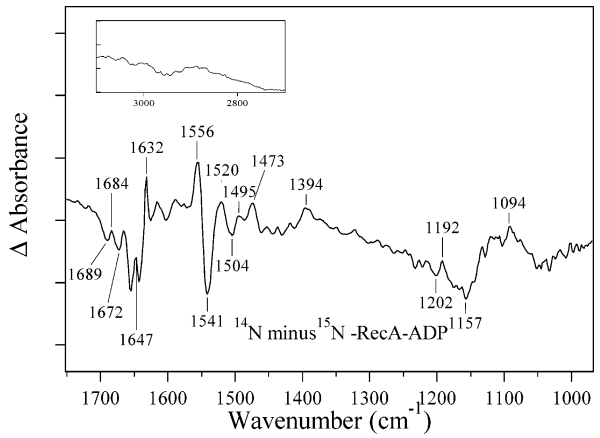

FIGURE 5: Double-difference spectrum generated using the same data shown in Figure 4 to isolate the differences between control and isotopically labeled protein samples. After normalization for protein content, the [^{15}N]RecA−ADP difference spectrum (Figure 4, solid line) was subtracted from the [^{14}N]RecA−ADP difference spectrum (Figure 4, dashed line). The tick marks on the *y* axis correspond 5×10^{-4} absorbance unit. The inset shows the 3000 cm^{-1} region of the same spectrum. The tick marks on the *y* axis of the inset correspond to 2×10^{-4} absorbance unit.

ADP and RecA−ATP complexes, they are centered around 1550 cm^{-1}. In spectra obtained on isotopically labeled RecA−ADP and RecA−ATP samples, they shift to around 1539 cm^{-1} with an additional shoulder at 1525 cm^{-1} in the RecA−ATP data. However, the data generated in the control samples reveal different peak absorbances for RecA−ATP (1549 cm^{-1}) and RecA−ADP (1556 cm^{-1}) spectra. This 7 cm^{-1} difference in the control samples suggests an additional contribution to the amide II region of the RecA−ATP spectra that shifts to the ∼1525 cm^{-1} region upon incorporation of ^{15}N.

ADP-Induced Changes in RecA Vibrations. Figure 4 shows the overlay of RecA−ADP spectra obtained for control and ^{15}N-labeled samples. The control spectrum shown in Figure 4 is essentially identical to previously published spectra using the same data acquisition technique (Figure 2), with the exception that the intensities of vibrations in Figure 4 are 2 times greater than those previously published (*29*). The increase in intensity is most likely due to a greater signal-to-noise ratio in the current data and the fact that three separate samples were used to generate the averaged spectra shown in Figure 4. Figure 5 (^{14}N minus [^{15}N]RecA−ADP) isolates vibrations influenced by isotopic labeling of the protein. The spectrum in Figure 5 was generated using amide I to normalize protein content between ^{14}N and ^{15}N samples and then subtracting the [^{15}N]RecA−ADP data (Figure 4, solid line) from the [^{14}N]RecA−ADP data (Figure 4, dashed line). The complex spectrum shown in Figure 5 reveals that ADP binding influences many nitrogen-containing amino acid vibrations and secondary structures. Many of the shifts and intensity differences previously observed in Figure 4 are more clearly elucidated in Figure 5. The lack of band broadening in the control RecA−ADP and [^{15}N]RecA difference data (Figure 4) suggests that the RecA−ADP conformational changes occurring over time have limited flexibility (*30*). The inset of Figure 4 shows the 3000 cm^{-1} region with distinct shifts of ∼10 cm^{-1} upon comparison of the control and ^{15}N samples. The negative 3300 cm^{-1} vibration and the positive vibrations centered around 3325 and 3257 cm^{-1} downshift approximately 10 cm^{-1} upon isotopic labeling as compared to the vibrations observed in the 2900−2970 cm^{-1} region that are not influenced by ^{15}N substitution. The inset of Figure 5 confirms that no isotopically induced shifts are observed in the 2800−3000 cm^{-1} region of the RecA−ADP spectrum as would be expected for C−H stretching vibrations (*39*).

The 1750−1350 cm^{-1} region in Figure 4 shows numerous shifts in intensity and frequency when the control and isotopically labeled samples are compared. Secondary structural changes are observed in the amide I region. β-Sheet structures (1625−1640 and 1675−1695 cm^{-1}), random coil structures (1640−1648 cm^{-1}), and α-helical structures (1648−1660 cm^{-1}) can dominate the 1600−1700 cm^{-1} region of the spectrum that also contains numerous nucleotide vibrations (*34*, *37*). The 1650−1630 cm^{-1} region in Figure 4 shows decreased intensity throughout the region when the labeled RecA−ADP minus RecA spectrum is compared to the unlabeled spectrum and contains numerous 2−3 cm^{-1} shifts that may be attributed to the amide I vibration (see Figure 1) (*40*). For example, the 1664 to 1662 cm^{-1} and 1647 to 1645 cm^{-1} shifts are consistent with the assumption that those vibrations originate from amide I contributions. Protein content was normalized between samples before the subtraction used to generate the spectrum in Figure 5, but the amount of nucleotide released in each experiment is slightly different. Thus, overall differences in intensity in the 1650 cm^{-1} region may arise from subtle differences in protein or nucleotide changes associated with improved binding in some samples. However, when nucleotide release is normalized between individual control and ^{15}N-labeled samples, prepared at the same time and on the same day and having nearly identical protein content, a double-difference spectrum similar to that shown in Figure 5 is observed (data not shown). Therefore, we can assume that most of the isotopically induced shifts and intensity variations

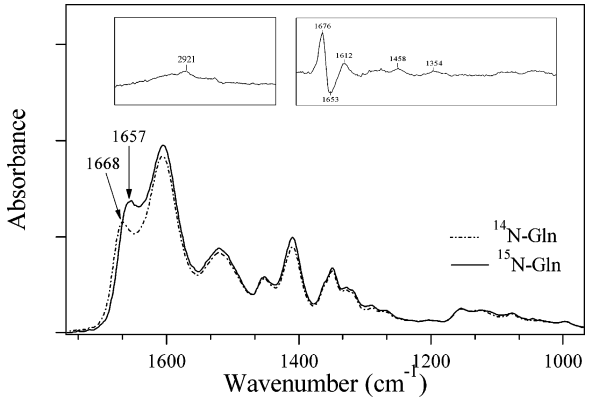

FIGURE 6: Absorbance spectra obtained for control L-glutamine (dashed line) and [*amide*-^{15}N]-L-glutamine (solid line) in the identical buffer used for RecA data, buffer M, at pH 7.5. Two separate samples were co-added for each spectrum. The tick marks on the *y* axis correspond to 10×10^{-3} absorbance unit. The insets (3100−2700 and 1750−1000 cm^{-1}) were generated by subtracting the ^{15}N spectrum (solid line) from the ^{14}N spectrum (dashed line) to isolate the differences associated with isotopic substitution.

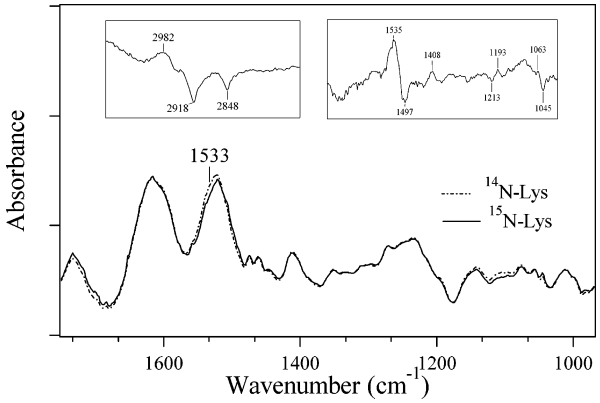

FIGURE 7: Absorbance spectra obtained for control L-lysine (dashed line) and [ϵ-^{15}N]-L-lysine (solid line) in the identical buffer used for RecA samples, buffer M, at pH 7.5. Two separate samples were co-added for each spectrum. The tick marks on the *y* axis correspond to 5×10^{-3} absorbance unit. The insets (3100−2700 and 1750−1000 cm^{-1}) were generated by subtracting the ^{15}N spectrum (solid line) from the ^{14}N spectrum (dashed line) to isolate the differences associated with isotopic substitution.

in the 1670−1630 cm^{-1} region seen in Figures 4 and 5 represent protein−backbone or side chain vibrations that are induced by ADP binding.

Of particular interest are the negative 1674 cm^{-1} vibration that decreases in intensity upon isotopic substitution (Figure 4) and the 1690 cm^{-1} region that also decreases in intensity while some intensities in this region are unchanged. This observation suggests that more than one protein or nucleotide vibration contributes to the signals in the control samples. Asn (C═O), Arg (C−N), and Gln (C═O) are all expected to have vibrations in this region (*35*, *41*) that should be influenced by ^{15}N incorporation. To investigate vibrations that may contribute to the observed spectra, we utilized isotopically labeled and control amino acid infrared spectra. The model Gln data presented in Figure 6 indicate a shift from 1668 to 1657 cm^{-1}. The inset of Figure 6 was generated by subtracting a [^{15}N]Gln spectrum from a [^{14}N]Gln spectrum and is therefore similar to the double-difference spectra shown in Figures 5 and 9. In addition to contributions from secondary structures and Asn, Arg, and Gln side chains, the 1600−1700 cm^{-1} region would also contain other nitrogen-containing side chain vibrations. For example, His (1631 cm^{-1}), Lys (1626−1629 cm^{-1}), Trp (1622 cm^{-1}), Pro (1616 cm^{-1}), Gln (1586−1610 cm^{-1}), and Asn (1612−1622 cm^{-1}) also absorb in this region and would be expected to shift upon ^{15}N incorporation (*35*, *41*, *42*).

The amide II vibration at 1556 cm^{-1} shifts to 1541 cm^{-1} in the ^{15}N difference spectrum. This shift is reflected in the sharp differential signal observed in Figure 5. Vibrations from lysine are also expected to absorb in this region around 1533 cm^{-1} (Figure 7, dashed line) and shift upon ^{15}N labeling (Figure 7, solid line). However, there is no clear change in the line shape of the differential signal at 1550 cm^{-1} upon labeling (compare dashed and solid lines in Figure 4) that may be expected if there were multiple nitrogen-containing vibrations contributing to this region. In addition, there are no clear isotopic shifts in the 2800−3000 cm^{-1} region of the RecA−ADP data (Figure 5 inset) such as those that are clearly observed in the lysine model data (Figure 7 inset). There is a lower-intensity 1473 cm^{-1} vibration in the control spectrum (Figure 4, dashed line) and new positive intensity around 1462 cm^{-1} in the ^{15}N-labeled spectrum (Figure 4, solid line). In addition, the double-difference spectrum in Figure 5 reflects these and other changes around 1495 and 1394 cm^{-1}. Numerous nitrogen-containing side chains have isotope-sensitive vibrations below 1500 cm^{-1}. For example, Trp (1496, 1462, and 1412−1435 cm^{-1}), His (1439 cm^{-1}), and Pro (1400−1465 cm^{-1}) all have side chain vibrations in the 1400−1500 cm^{-1} region (*35*, *42*). A positive vibration in the control RecA−ADP spectrum at 1394 cm^{-1} in Figure 4 is less intense in the [^{15}N]RecA−ADP spectrum. Typically, most of the vibrations present in the 1270−970 cm^{-1} region arise from nucleotide phosphate vibrations that tend to dominate this region of the spectra, as seen in Figure 3 (*43*). However, we observed some small differential signals at 1200, 1157, and 1094 cm^{-1} (Figure 5) that are only isolated in the double-difference data. These differential signals are consistent with protein C−N vibrations such as those found in Arg and Lys side chains (Figure 7) (*44*).

ATP-Induced Changes in RecA Vibrations. Figure 8 shows the overlay of RecA−ATP spectra obtained on control (dashed line) and ^{15}N-labeled (solid line) RecA samples. Although the current RecA−ADP data are nearly identical to those previously published, the RecA−ATP data presented here show some significant changes in the amide I region (Figure 8, dashed line) when we compare it to our previous results using a similar data acquisition procedure (*29*) but different RecA sources. Prior to averaging, each of the single difference spectra used here had approximately twice the intensity in the amide II region as the previously published spectra. We do not observe the time-dependent transition from negative to positive contributions in the 1670−1680 cm^{-1} region in the data presented here that we observed previously (*29*). Figure 3 ([^{14}N]RecA−ATP, dashed line) shows that we observe positive 1670−1680 cm^{-1} vibrations that continue to grow more positive over time. In addition, the previously observed 1653 cm^{-1} peak is now a shoulder on a more intense vibration centered at 1662 cm^{-1} (Figure 8, dashed line). However, the vibrations below 1600 cm^{-1} are nearly identical in the present control RecA−ATP spectrum and the previously published data (*29*).

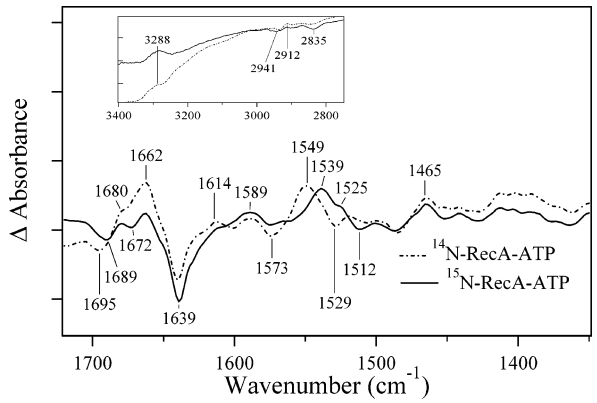

FIGURE 8: Difference spectra obtained by ratioing the spectrum taken at 40 min to the spectrum taken immediately after photolysis. RecA−ATP minus RecA difference spectra obtained on samples that contained caged ATP and either control, [^{14}N]RecA (dashed line) or ^{15}N-labeled RecA (solid line). Each spectrum is an average of three spectra obtained on three different samples. To compare intensities of the various spectra, the amide I vibration of averaged absorbance spectra was used to normalize for protein content. The tick marks on the *y* axis correspond to 1×10^{-3} absorbance unit. The inset shows the 3000 cm^{-1} region of the same spectra: [^{14}N]RecA (dashed line) and ^{15}N-labeled RecA (solid line). The tick marks on the *y* axis of the inset correspond to 1×10^{-3} absorbance unit.

The inset of Figure 8 (RecA−ATP) shows the 3300 cm^{-1} region that does not contain the distinct changes observed in the Figure 4 inset (RecA−ADP). However, the insets of Figures 8 and 9 do show isotopically induced shifts in the 2800−3000 cm^{-1} region that are unique to the RecA−ATP complex and similar to those observed in the Lys model data (Figure 7 inset). In addition, the vibrations present in the 1750−1350 cm^{-1} region of the spectra are also less distinct than those observed in Figure 4, especially when the control samples are being compared (Figures 4 and 8, dashed lines). This was also true in the previous data obtained for samples in Hepes buffer (*29*), yet the RecA−ATP data obtained for samples in Tris buffer showed vibrations that were slightly more distinct (*28*). The broader line shapes of RecA−ATP data obtained in Hepes buffer correlated with the activity assays, implying that 100× Hepes buffer supports ATP hydrolysis in the absence of DNA. Interestingly, only negligible hydrolysis was observed in the presence of 100× Tris buffer conditions used to mimic the infrared conditions that yielded more distinct vibrations (*28*, *29*). Since the width of the vibrations is a measure of conformational freedom, the structures associated with the RecA−ATP complex may be somewhat more flexible than those present in the RecA−ADP structure (*30*). Also striking is the fact that fewer distinct isotopic shifts are observed in the 1750−1350 cm^{-1} region in the RecA−ATP spectra (Figure 8) than in the RecA−ADP spectra (Figure 4). Figure 8 reveals some shifts that arise from incorporation of ^{15}N into RecA. For example, a negative 1695 cm^{-1} vibration observed in the control shifts to 1689 cm^{-1} in the isotopically labeled RecA−ATP spectrum. This vibration present in the RecA−ATP spectrum must be different than that observed in the RecA−ADP data (Figure 4), since the 1691 cm^{-1} vibration in Figure 4 does not show any substantial shifts upon isotope incorporation. In addition, a positive 1672 cm^{-1} contribution (Figure 8, dashed line) is no longer evident in the [^{15}N]RecA−ATP spectrum; instead, a negative vibration is observed upon isotopic labeling (Figure 8, solid line) that looks more similar to the RecA−ADP control data (Figure 4, dashed line). There seem to be some subtle differences in the shape and intensity of vibrations in the 1600−1660 cm^{-1} region that are difficult to discern in this crowded region of the spectra. For example, the control spectrum has increased positive intensity around 1662 cm^{-1}, and the ^{15}N spectrum has a different line shape in the 1612−1630 cm^{-1} region. In addition, the control RecA−ATP spectrum contains a negative vibration at 1573 cm^{-1} that is not evident in the [^{15}N]RecA−ATP spectrum. Both His (1575−1594 cm^{-1}) and Gln (1586−1610 cm^{-1}) have infrared vibrations that would be expected to shift in this region (*35*, *41*).

One of the more pronounced isotope-induced shifts is most easily observed when comparing multiple data sets. Interestingly, we observe that the amide II vibration is downshifted ∼7 cm^{-1} in the RecA−ATP control difference spectrum (Figure 8, dashed line) when compared to the RecA−ADP control spectrum (Figure 4, dashed line). However, when comparing [^{15}N]RecA−ATP and [^{15}N]RecA−ADP data, we observe an only 2 cm^{-1} difference in the amide II vibration (Figures 4 and 8, solid lines). Furthermore, isotopic labeling results in a new 1525 cm^{-1} vibration in the RecA−ATP spectrum (Figure 8, dashed line). These differences are perhaps more clearly observed in Figures 3 and 10. Comparison of the line shapes of the control and ^{15}N-labeled RecA−ATP difference spectra (Figure 8) suggests that the positive feature at 1549 cm^{-1} present in the control sample is not entirely dominated by the amide II vibration as is more likely the case in the RecA−ADP spectrum shown in Figure 4. Instead, a second positive feature shifts to ∼1525 cm^{-1} after labeling. These differences could be due to the presence of additional amino acid vibrations in the RecA−ATP data. The amino acid side chain that would most likely give rise to this additional vibration in this region is lysine (Figure 7). However, a vibration at 1553 cm^{-1} has been unambiguously assigned to an Arg in bacteriorhodopsin that is perturbed during the photocycle (*45*). The region between 1500 and 1260 cm^{-1} is similar in both the [^{14}N]- and [^{15}N]RecA−ATP samples with the exception that there is additional intensity in control samples in the 1370−1415 cm^{-1} region.

To isolate vibrations affected by the isotopic substitution, [^{14}N]RecA−ATP minus [^{15}N]RecA−ATP data were generated. The spectrum shown in Figure 9 reveals broad positive vibrations at 1687, 1670, and 1662 cm^{-1}. However, the corresponding negative vibrations for the [^{15}N]RecA are not easily resolved due to the spectral complexity of this region. Differential vibrations at 1645 and 1637 cm^{-1} are also resolved in addition to positive vibrations at 1614 and 1589 cm^{-1}. The differential signal around 1552−1531 cm^{-1} is much broader than that observed in Figure 5. Other differential signals are observed around 1495−1483 and 1452−1439 cm^{-1}. The 1320−970 cm^{-1} region shows numerous signals that are influenced by ATP binding and are not observed in the RecA−ADP data. Although most of the vibrations present in the 1270−970 cm^{-1} region (Figure 3) typically arise from nucleotide phosphate vibrations (*43*) in Figure 9, we observe distinct differential signals around 1261−1238, 1175−1144, and 1134−1124 cm^{-1} that correspond to protein vibrations affected by isotopic substitution. Arg and Lys C−N vibrations are reasonable candidates for

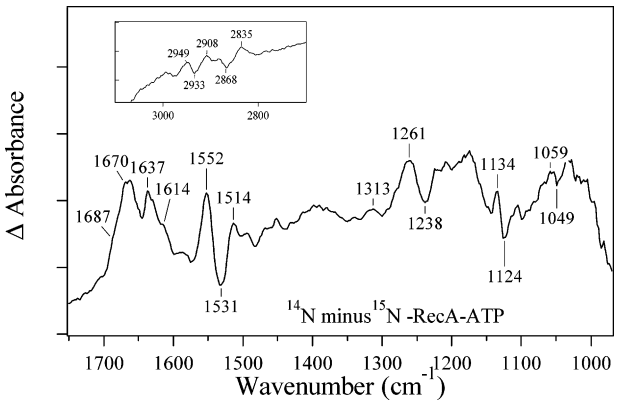

FIGURE 9: Double-difference spectrum generated using the same data shown in Figure 8 to isolate the differences between control and isotopically labeled protein samples. After normalization for protein content, the [^{15}N]RecA−ATP difference spectrum (Figure 8, solid line) was subtracted from the [^{14}N]RecA−ATP difference spectrum (Figure 8, dashed line). The tick marks on the *y* axis correspond to 5×10^{-4} absorbance unit. The inset shows the 3000 cm^{-1} region of the same spectrum. The tick marks on the *y* axis of the inset correspond to 2×10^{-4} absorbance unit.

the vibrations in the 1250−1000 cm^{-1} region that are influenced by ^{15}N incorporation (Figure 7 inset), yet Trp and His vibrations may also contribute in this region (*35*, *44*).

DISCUSSION

For many years, research on RecA has focused on identifying protein−protein, protein−nucleotide, and protein−DNA interactions that result from the binding of ATP, ATP analogues, and ADP. However, many questions concerning how ATP uniquely interacts with RecA to form a high-affinity protein complex and how ATP hydrolysis is coupled to DNA strand exchange remain unanswered. In efforts aimed at identifying key protein−nucleotide and protein−protein interactions associated with nucleotide binding, we have utilized difference FTIR to study binding of ADP and ATP to wild-type RecA in the absence of DNA. Here, we have focused on isolating the vibrational changes associated with the allosteric regulation of RecA in the absence of DNA. The method of data analysis used to generate the difference spectra shown here does not require the subtraction of contributions from the photolytic release of the cage as performed previously (*28*, *29*), thus allowing a more accurate analysis of the 1520 and 1347 cm^{-1} regions of the spectra that are typically dominated by vibrations arising from the photolytic release of the cage (*28*). This method of data accumulation allows us to examine slow structural changes or residual nucleotide binding without the broad background vibrations associated with assembly and disassembly of the protein filament or perturbations in the nucleotide that may occur immediately following photolytic release. Figure 3 shows that the RecA structure continues to change over time under the conditions utilized in these experiments. These slow changes could result simply from the sample conditions utilized in our experiments. Other possible reasons for the slow structural changes include the observation of cooperativity between RecA monomers or an isomerization of the RecA−nucleotide complexes similar to that which has previously been observed for the RecA−DNA−ATPγS complexes (*46*). Interestingly, although the RecA−ADP and RecA−ATP structures are distinct, in each case a continuous increase in intensity over time is observed. This result indicates that most of the RecA monomers are adopting a single, predominant conformation over time that is unique to the bound nucleotide.

It is important to note that partial dehydration of the RecA samples results in a protein film with very high concentrations of protein (∼10 mM) and buffer salts, including high concentrations of $MgCl_2$ (∼100 mM). It is known that increasing Mg^{2+} and protein concentrations, along with low temperatures, stabilizes the formation of RecA filaments (*47*, *48*). Although previous EM experiments were performed with millimolar concentrations of $MgCl_2$ and 1−200 μM RecA, these results suggest that the RecA in our samples would originally be found in aggregates of filamentous structures (*47*, *48*) with very little of the RecA found in the ringlike structures observed at lower protein and $MgCl_2$ concentrations (*47*, *48*). In addition, activity assays performed under buffer conditions that mimic the infrared conditions used here (*29*) imply that the RecA infrared samples may exist in a more extended or active conformation that is able to hydrolyze ATP in the absence of DNA (*7*, *8*). The low temperatures in our experiments may preclude any substantial amount of ATP hydrolysis during our experiments but would allow for cooperative protein conformational changes or isomerization reactions to occur over time.

Difference spectra contain a plethora of information concerning changes in the protein and nucleotide and reveal changes that occur throughout the entire protein. Many vibrations arising from backbone conformations and side chains can overlap and make spectral analysis more difficult (*30*). The RecA−ADP minus RecA and RecA−ATP minus RecA difference spectra reflect the net vibrational changes associated with nucleotide binding (*30*). We performed experiments on control and globally ^{15}N-labeled RecA to aid in the interpretation of the difference spectra associated with binding of nucleotide to RecA. Many of the vibrations previously observed (*28*, *29*) that could not be directly attributed to RecA due to the possible contributions of the nucleotide are now identified as protein vibrations. The combination of model compound studies and isotopic labeling helps in the unraveling of the complex spectral regions and in better understanding important structures associated with the ATP- and ADP-bound forms of RecA. Protein vibrations affected by isotopic labeling could include both amino acid side chains and secondary structural changes. Mutagenesis and crystallography studies (reviewed in ref *12*) have suggested key roles for amino acids such as Gln, Lys, Arg, Asp, Pro, and His in binding nucleotides and transmitting information throughout the RecA protein. The vibrational shifts due to ^{15}N labeling in the difference data in Figures 4 and 5 reveal the possible involvement of Arg, Gln, His, Pro, Trp, and Asn upon binding of ADP to RecA. The isotopically induced vibrational shifts in Figures 8 and 9 show the possible involvement of Lys, Arg, Gln, Trp, and His upon binding of ATP to RecA.

The most interesting vibrations that could be associated with allosteric regulation of RecA are those vibrations that are unique to either the ATP- or ADP-bound states of RecA and are affected by isotopic substitution such that they can be definitely assigned to changes in protein structure. The comparison of all of the RecA−ATP and RecA−ADP data (Figures 3 and 10) gives unique insights into the origin of

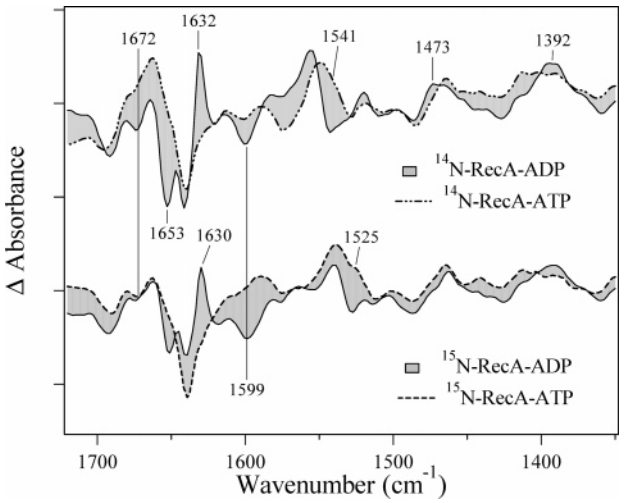

FIGURE 10: Comparison of RecA−ATP minus RecA and RecA−ADP minus RecA difference spectra. Difference spectra obtained by ratioing the spectrum taken at 40 min to the spectrum taken immediately after photolysis. RecA−nucleotide minus RecA difference spectra obtained on samples that contained caged ATP (dashed lines) or caged ADP (solid lines) and either control, [^{14}N]RecA, or ^{15}N-labeled RecA. Each spectrum is an average of three spectra obtained on three different samples. To compare intensities of the various spectra, the amide I vibration of averaged absorbance spectra was used to normalize for protein content. The tick marks on the *y* axis correspond to 1×10^{-3} absorbance unit.

some of the vibrations present in our data. Overall, the [^{14}N]- minus [^{15}N]RecA−ADP data contain sharper differential signals in the 1750−1350 cm^{-1} region than those observed in the [^{14}N]- minus [^{15}N]RecA−ATP data (Figures 5 and 9). Distinct vibrations around 3300 cm^{-1} (Figure 4 inset compared to Figure 8 inset) in the RecA−ADP spectrum are associated with N−H stretching vibrations and are not obvious in the RecA−ATP data. Unique isotopically induced shifts are observed in the RecA−ATP data that are absent in the RecA−ADP data (Figure 5 inset compared to Figure 9 inset). Thus, it is clear that RecA−ADP and RecA−ATP conformations have distinct structures.

The RecA−ADP data clearly show unique negative ∼1651 cm^{-1} and positive ∼1631 cm^{-1} vibrations with small 1−2 cm^{-1} shifts upon ^{15}N incorporation, implying that these vibrations arise from secondary structural changes (*34*). These vibrations are consistent with the disappearance of α-helix and the formation of a unique *β*-structure upon binding of ADP to RecA. However, a lysine, histidine, or arginine side chain could also contribute to the positive 1631 cm^{-1} vibration (*35*, *41*, *44*). The double-difference spectrum shown in Figure 5 reveals that some of the 1631 cm^{-1} vibration may shift and show up as a small negative peak at 1626 cm^{-1}. Additionally, both control RecA−ATP and RecA−ADP spectra contain negative vibrations around 1640 cm^{-1} (Figure 10), the magnitudes of which decrease upon isotopic substitution, yet neither the RecA−ADP nor the RecA−ATP difference spectra show new intensity associated with ^{15}N-induced vibrational shifts. Unlike the RecA−ADP data, the RecA−ATP data (Figure 8) suggest that the random coil or *β*-structure content (1639 cm^{-1}) decreases and α-helical structure content (1650−1665 cm^{-1}) increases when ATP is bound.

The difference data shown in Figure 4 display negative contributions around 1690 cm^{-1} in the RecA−ADP spectrum that are consistent with the disappearance of *β*-structure, perturbation of the nucleotide, or different interactions between amino acid side chains such as Arg, Gln, and Asn. Two vibrations may give rise to the negative intensity around 1690 cm^{-1} in the RecA−ADP data, since the vibration at this position decreases in intensity upon isotopic substitution, whereas the remaining intensity is centered at 1691 cm^{-1} in the [^{15}N]RecA−ADP data (Figure 4). However, the RecA−ATP data (Figure 8) show a negative vibration around 1695 cm^{-1} that shifts to 1689 cm^{-1} upon isotopic substitution. This 6 cm^{-1} shift suggests that the origin of the 1695 cm^{-1} vibration in the RecA−ATP spectrum (Figure 8) is from one of the suggested side chains or a unique protein structure that does not contribute to the RecA−ADP data (Figure 10).

A key difference between the RecA−ADP and RecA−ATP spectra centers around 1673 cm^{-1}, where a positive vibration is affected by ^{15}N labeling in RecA−ATP data and a negative vibration decreases in intensity upon labeling in the RecA−ADP spectrum (Figure 10). This remaining intensity in the [^{15}N]RecA−ADP spectrum may suggest that both amino acid side chain vibrations (such as Asn, Arg, or Gln) and *β*-structure or nucleotide changes could contribute to the negative 1674 cm^{-1} [^{14}N]RecA−ADP vibration (Figure 4). The positive 1672 cm^{-1} vibration in the control RecA−ATP spectrum shifts upon isotopic substitution and results in a negative 1672 cm^{-1} signal in the [^{15}N]RecA−ATP spectrum that resembles that observed in the control RecA−ADP spectrum (Figure 10). The negative 1672 cm^{-1} vibration in the RecA−ATP data may arise from a shift induced by isotopic incorporation. Another possibility is that part of the negative component around 1673 cm^{-1} could be similar for binding of both ATP and ADP to RecA, yet it is only observed in the RecA−ATP spectrum when a positive contribution shifts out of this region (Figure 10). Therefore, part of this negative vibration may arise from a nucleotide perturbation, a protein side chain, or an element of secondary structure that is similarly affected by binding of both ATP and ADP to RecA. Importantly, the positive 1672 cm^{-1} vibration is observed only in the control RecA−ATP spectra, suggesting that the origin of this vibration is a key structure involved in alternating between low- and high-affinity DNA protein structures. The difference spectra imply a unique interaction between ATP and either Gln, Arg, or Asn (*35*, *41*). Gln194 is a strong candidate for this interaction since it protrudes into the nucleotide-binding site and has been implicated in mediating the allosteric regulation induced by binding of ATP to RecA (*17*, *27*). However, Arg196 has also been suggested to be a key amino acid involved in nucleotide binding and hydrolysis (*23*, *24*). It is possible that Arg, Gln, and Lys residues may act as sensor residues that are close to the nucleotide-binding site but ultimately result in the transfer of information through the protein, as initially proposed for Gln194 (*17*, *27*). Information transfer between RecA monomers may also occur through arginine side chains. Ye et al. (*50*) note that "arginine fingers" are a common mechanism for communication between RecA-like domains found in other proteins such as F1ATPase.

The RecA−ADP data also suggest that a Gln, Arg, or Asn adopts a unique, altered conformation and could act as a sensor that is influenced by ADP binding since part of the negative intensity at 1674 cm^{-1} in the control sample disappears in the ^{15}N-labeled RecA−ADP spectrum (Figure

4). Control and ^{15}N-labeled model infrared studies of Arg reveal 4−9 cm^{-1} shifts in C−N vibrations around 1656, 1614, 1440, 1170, and 1087 cm^{-1} upon ^{15}N labeling (*44*). The spectrum in Figure 5 shows isotopically induced changes in nearly all of the regions where Arg side chains would be expected to shift, including differential signals around 1654, 1616, 1200, 1157, and 1094 cm^{-1}. The model Gln data presented in Figure 6 show a shift from 1668 to 1657 cm^{-1} upon ^{15}N labeling. A corresponding shift in the protein data presented in Figure 4 would result in a new negative contribution around 1663 cm^{-1} that is difficult to discern in the [^{15}N]RecA−ADP spectrum due to the more intense positive vibration around 1662 cm^{-1}. According to the double-difference model data presented in Figure 6, Figure 5 should show a positive vibration 23 cm^{-1} lower than the negative vibration around 1672 cm^{-1} associated with the RecA−ADP complex if the data supports the involvement of glutamine. Figure 5 reveals a positive vibration at 1647 cm^{-1} that is consistent with this interpretation, but this is a very crowded spectral region.

The positive ∼1670 cm^{-1} contribution and the vibrations in the 2800−3000 cm^{-1} region in the RecA−ATP data clearly indicate distinctive side chain conformations in the RecA−ATP structure. RecA−ATP minus RecA−ADP double-difference spectra generated from the control data in this paper (data not shown) are very similar to that previously published (*29*) and show positive vibrations around 1689, 1672, 1653, and 1641 cm^{-1}, while the [^{15}N]RecA−ATP minus RecA−ADP data (not shown) show negative contributions in all of these regions, except that the 1653 cm^{-1} vibration shifts ∼2 cm^{-1}. The double-difference data (not shown) and comparison of the spectra in Figure 10 support the suggestion that there is increased α-helical structure content in the RecA−ATP structure and that the other vibrations in the 1640−1690 cm^{-1} region arise from the probable side chains discussed above. Most likely, the side chain vibrations in the 1670−1690 cm^{-1} region are indicative of sensor residues that adopt alternate conformations in the RecA−ATP and RecA−ADP structures.

Another important difference between infrared data obtained for the two nucleotide-bound states of RecA is a positive 1549 cm^{-1} vibration in the control RecA−ATP spectrum that most likely contains contributions from amide II (Figure 8, dashed line). Interestingly, this vibration shifts to 1541 cm^{-1} (with a shoulder at 1525 cm^{-1}) in the [^{15}N]RecA−ATP spectrum (Figure 10). The amide II vibration associated with the RecA−ADP complex (1556 cm^{-1}) shows a shift similar to that of the 1539 cm^{-1} vibration but does not contain a shoulder at 1525 cm^{-1}. Most likely, the broad RecA−ATP vibration that is centered around 1549 cm^{-1} contains a contribution around the 1530 cm^{-1} region of the RecA−ATP spectrum that is in addition to the amide II vibration. This additional contribution is revealed by isotopic labeling and suggests that a different secondary structure or side chain has a unique conformation in the RecA−ATP complex. The most likely amino acids to give rise to this vibration in the Rec−ATP spectra include Lys (Figure 7) and Arg, suggesting a crucial role for these side chains in the allosteric regulation of RecA (*35*, *41*, *45*). The lysine absorbance spectra (Figure 7) support the possibility that a lysine side chain is affected by ATP binding. Vibrations in the 2800−3000 cm^{-1} region of the lysine and RecA−ATP spectra shift upon ^{15}N incorporation. The origin of these vibrations remains unclear. An N−H stretch that is very strongly hydrogen bonded may result in vibrations that are significantly lower in magnitude than those observed for the RecA−ADP complex. However, spectra obtained on the lysine model compounds in deuterium oxide showed similar vibrations (data not shown), thus eliminating the possibility that strongly hydrogen bonded N−H groups in the model compounds give rise to these signals. The lack of any similar vibrations in the glutamine spectra may suggest that the 2800−3000 cm^{-1} vibrations could arise from coupled C−H and C−N vibrations or combinations of fundamental vibrations. Although we are not certain about the origin of the vibrations around 2900 cm^{-1}, it is clear that the RecA−ATP spectra have a signature that is not found in the RecA−ADP spectra but is similar to the vibrations that are observed in the lysine spectra. However, we cannot eliminate the possibility that arginine side chains or secondary structural changes contribute to changes in the 2900 cm^{-1} region of the RecA−ATP data. Previous studies in our laboratory show unique contributions around 1541 cm^{-1} associated with the RecA−ATP complex that are influenced by deuterium exchange and support the data presented here (*29*). Mutations at lysine 72 result in a protein that is able to bind but not hydrolyze ATP (*26*) and imply a crucial role for this amino acid that is located in the nucleotide-binding site. Although the RecA−MnAMP-PNP crystal structure complex is in a compressed conformation, the authors constructed a model of the active form that suggests that lysines 248 and 250 on the adjacent RecA monomer are near the MnAMP-PNP phosphates in the nucleotide-binding site (*20*). The infrared data associated with the RecA−ATP complexes are also consistent with the idea that a specific change in conformation of one or more lysine side chains is crucial for the adoption of the high-affinity RecA structure. In fact, the more complex pattern observed in the 2900 cm^{-1} vibration of the RecA−ATP data (Figure 9 inset) as compared to the pattern observed in the lysine model data (Figure 7 inset) could indicate more than one side chain is contributing to changes in this region. In addition, a positive vibration centered at 1394 cm^{-1} in the RecA−ADP spectrum (Figure 4, dashed line) and the lack of a vibration in this region of the RecA−ATP spectrum (Figure 8) could implicate movement of Gln, Pro, or Trp when the RecA−ADP structure is adopted (*35*). Pro67 is located in the P-loop motif, and studies of Pro67 mutants have shown that it is a functionally important residue involved in modulating NTP specificity as well as coprotease and recombination activities (*51*, *52*). Overall, the large influence that global nitrogen labeling of RecA has on the difference spectra suggests that many of the amino acids that control the allosteric regulation of RecA contain nitrogen in their side chains.

Binding of nucleotide to RecA influences numerous monomer−monomer interactions in a cooperative fashion. Therefore, it is interesting to explore the differences between RecA−ATP and RecA−ADP structures at the subunit interfaces. This comparison may provide valuable insights into the allosteric regulation of RecA. Crystal structures predict that our data should reveal small differences that arise from the nucleotide-binding regions of the RecA−ATP and RecA−ADP structures. Key amino acid vibrations and secondary structural changes could arise from interactions

at the monomer−monomer interface in addition to changes that occur in the binding pocket of the RecA protein. Unique differences associated with the RecA−ATP complex include the possible involvement of Gln, Asn, or Arg (1672 cm^{-1}, Figure 10), Lys and Arg (2900 cm^{-1} region and 1530 cm^{-1}, Figure 8, dashed line), and unique α-helical and β-structures in the RecA−ATP complex (∼1650−1690 cm^{-1}). The RecA−ADP data show vibrations that may be associated with β-structure, Arg or Lys (∼1630 cm^{-1}), and side chain conformations of Gln (negative at 1674 cm^{-1}), His, Pro, and Trp (1473 and 1394 cm^{-1}) that are specific to the inactive conformation of RecA. Mutagenesis and crystallographic studies reviewed by McGrew and Knight reveal that numerous side chain interactions occur at the monomer−monomer interface (*12*). The most common interactions of interest often occur between a Lys, Arg, His, or Asn that interacts with a Glu or Asp residue on the neighboring subunit (*12*). For example, mutations at Lys6 and Arg28 in the N-terminal region of RecA disrupt oligomer formation and implicate them in cross-subunit interactions that are important to the stability of the inactive form of RecA (*53*, *54*). Additional salt bridges in the RecA−ADP data should also be associated with unique vibrations consistent with changes in Asp and Glu residues that are not influenced by ^{15}N incorporation. Figures 4 and 10 show that the RecA−ADP data contain unique positive vibrations in the 1560−1580 and 1400 cm^{-1} regions of the spectra and a unique negative vibration around 1599 cm^{-1} that do not shift upon ^{15}N labeling but were influenced by deuterium exchange (*29*). Thus, the data are consistent with the possibility that deprotonated Asp or Glu (COO^-) vibrations are influenced by nucleotide binding and could be interacting with the N−H vibrations clearly observed in the RecA−ADP data (Figure 4) (*35*, *41*).

The difference data presented here support the notion that the RecA−ADP complex is more rigid than the RecA−ATP complex. The RecA−ADP data have more defined vibrations in contrast with the ATP difference data that contain broader vibrations. Although there may not be a large change in bandwidth, the data seem to suggest increased flexibility in the RecA−ATP structure. An increase in flexibility or a slightly more heterogeneous RecA−ATP population would explain subtle differences between RecA−ATP minus RecA and RecA−ADP minus RecA data obtained in our lab (*28*, *29*). The difference spectra result from contributions of all RecA monomers that bind nucleotide. A very heterogeneous RecA−ATP sample may be expected to result in decreased signal-to-noise difference spectra if there were significant populations of multiple conformations. The possibility also exists that there are fewer nitrogen-containing side chain vibrations influenced by ATP binding or that protein or nucleotide structural changes overshadow amino acid side chain vibrations. The N−H vibrations that are unique to the RecA−ADP form (Figure 4 inset) and shift upon isotopic incorporation are of particular interest. The N−H vibrations are not clearly resolved in the RecA−ATP data (Figure 8). The lack of N−H vibrations may arise from heterogeneous broadening of the vibrations or the absence of the interactions that give rise to the vibrations present in the RecA−ADP data. The vibrations in the 3300 cm^{-1} region of the RecA−ADP spectra could arise from N−H groups that are involved in locking RecA into a less flexible, more compact conformation with a lower affinity for DNA. The observed isotopically induced shifts (Figure 4) clearly indicate that distinctive protein N−H vibrations are involved in the formation of the RecA−ADP complex. The changes in the N−H vibrations induced by nucleotide binding are consistent with vibrations involved in additional hydrogen bonding interactions in the RecA−ADP complex. These N−H vibrations may arise from side chains involved in forming salt bridges between monomers or interactions within the binding site of the RecA−ADP complex. Recently determined structures of the compressed inactive filament of RecA show that movement is greatest for β-strands at the C-terminal domain (*19*) and could explain the unique RecA−ADP and unique RecA−ATP vibrations consistent with β-structure. Studies on *E. coli* RecA have suggested the importance of the C-terminal domain in mediating allosteric transitions through interactions with the neighboring monomer (*13*−*16*). In addition, studies have shown that ADP stabilizes contacts between the central and C-terminal domains that are weakened by ATP (*55*). EM reconstructions have shown the greatest amount of disorder in the C-terminal domain occurs when ATP analogues are bound to RecA (*13*) in contrast to the more ordered structure of the RecA−ADP filaments. Fluorescence experiments that monitored DNA flexibility revealed ATP-induced flexibility in RecA−DNA filaments that contrast with a more rigid RecA−DNA−ATPγS filament (*56*). The infrared data presented here suggest that more flexible RecA−ATP filaments are present in the absence of DNA. The RecA−ADP filaments have a greater number of discrete vibrational changes and provide additional evidence for the increased number of contacts within or between the RecA−ADP filaments.

SUMMARY

The difference infrared data associated with binding of ATP and ADP to control and ^{15}N-labeled RecA show numerous vibrations that can now be unambiguously assigned to protein vibrations. Activity assays performed under conditions that mimic the salt concentrations in the infrared samples show that the RecA is active in the absence of DNA and imply a more active or extended conformation of RecA filaments. Each complex, RecA−ATP and RecA−ADP, contains unique secondary structures (α-helix and β-sheet) and side chain interactions influenced by ^{15}N labeling of the protein. The infrared data presented here give rare, molecular-level information about the structure of RecA bound to ATP. The data suggest that RecA−ADP complexes may be less flexible than the RecA−ATP complexes and that the ADP complexes contain vibrations consistent with an increased number of side chain interactions such as those involved in salt bridges between the RecA monomers. The inactive, more compact RecA−ADP conformation could result from the increased number of interactions between monomers or distinct structural changes transmitted throughout the protein via sensor amino acids near the nucleotide-binding site. Specific changes in N−H stretches occur upon ADP binding and are not evident in the RecA−ATP complex. The infrared data suggest that Arg, Gln, or Asn may be uniquely altered in both the ADP- and ATP-bound states of RecA. The structure or residue giving rise to the positive 1672 cm^{-1} vibration in the RecA−ATP data contains nitrogen and is important in the allosteric regulation of RecA. One of the most likely candidate side chains for this vibration is a Gln,

possibly Gln194 that is located in the binding site. The model spectra obtained for isotopically labeled glutamine support the possibility that a Gln side chain could give rise to this unique vibration. Furthermore, the RecA−ATP data contain multiple vibrations consistent with the involvement of Lys and Arg side chains that are exclusive to the RecA−ATP complex. The Lys and Arg side chains may be involved in important interactions in the nucleotide-binding site or between RecA monomers that are observed only in the more active conformation of RecA. The model data support the possibility that Lys side chains are involved in the allosteric regulation of RecA. Future difference infrared experiments with RecA mutants could result in more detailed information about the pathway associated with the transmission of information from the nucleotide-binding site to interactions between RecA monomers. Infrared spectroscopy provides the ability to follow molecular-level changes that occur in the protein and nucleotide over time. The slow changes revealed in the time-dependent data are consistent with cooperative interactions between monomers or the slow isomerization of RecA−nucleotide complexes as they move toward a common structure that is dictated by the bound nucleotide. Interestingly, these slow, continuous changes in protein structure occur when either nucleotide binds, yet result in distinct protein conformations. The infrared data obtained for isotopically labeled protein will aid in the interpretation of subsequent work. Future attempts to answer the long-standing question of how ATP hydrolysis influences protein structures to promote DNA strand exchange will result from experiments that allow us to isolate protein and nucleotide vibrations that are coupled during ATP hydrolysis.

ACKNOWLEDGMENT

The *E. coli* STL327 strain and pAIR79 plasmid were the generous gift of Dr. Michael Cox.

REFERENCES

1. Bianco, P. R., Tracy, R. B., and Kowalczykowski, S. (1998) DNA strand exchange proteins: A biochemical and physical comparison, *Front. Biosci. 3*, d570−d603.
2. Cox, M. M. (2003) The bacterial RecA protein as a motor protein, *Annu. Rev. Microbiol. 57*, 551−577.
3. Brendel, V., Brocchieri, L., Sandler, S. J., Clark, A. J., and Karlin, S. (1997) Evolutionary comparisons of RecA-like proteins across all major kingdoms of living organisms, *J. Mol. Evol. 44*, 528−541.
4. Roca, A. I., and Cox, M. M. (1997) RecA Protein: Structure, Function, and Role in Recombinational DNA Repair, *Prog. Nucleic Acid Res. Mol. Biol. 56*, 129−223.
5. Walker, J. E., Saraste, M., Runswick, M. J., and Gay, N. J. (1982) *EMBO J. 1*, 945−951.
6. Menetski, J. P., and Kowalczykowski, S. C. (1985) Interaction of recA protein with single-stranded DNA. Quantitative aspects of binding affinity modulation by nucleotide cofactors, *J. Mol. Biol. 181*, 281−295.
7. Pugh, B. F., and Cox, M. M. (1988) High salt activation of recA protein ATPase in the absence of DNA, *J. Biol. Chem. 263*, 76−83.
8. Ellouze, C., Takahashi, M., Wittung, P., Mortensen, K., Schnarr, M., and Norden, B. (1995) Evidence for elongation of the helical pitch of the RecA filament upon ATP and ADP binding using small-angle neutron scattering, *Eur. J. Biochem. 233*, 579−583.
9. Roca, A. I., and Singleton, S. F. (2003) Direct evaluation of a mechanism for activation of the RecA nucleoprotein filament, *J. Am. Chem. Soc. 125*, 15366−15375.
10. Egelman, E. H. (1993) What do X-ray crystallographic and electron microscopic structural studies of the RecA protein tell us about recombination? *Curr. Opin. Struct. Biol. 3*, 189−197.
11. Yu, X., VanLoock, M. S., Yang, S., Reese, J. T., and Egelman, E. H. (2004) What is the strucure of the RecA-DNA filament? *Curr. Protein Pept. Sci. 5*, 73−79.
12. McGrew, D. A., and Knight, K. L. (2003) Molecular design and functional organization of the RecA protein, *Crit. Rev. Biochem. Mol. Biol. 38*, 385−432.
13. VanLoock, M. S., Yu, X., Yang, S., Lai, A. L., Low, C., Campbell, M. J., and Egelman, E. (2003) ATP-mediated conformational changes in the RecA filament, *Structure 11*, 187−196.
14. Eggler, A. L., Lusetti, S. L., and Cox, M. M. (2003) The C terminus of the *Escherichia coli* RecA protein modulates the DNA binding competition with single-stranded DNA-binding protein, *J. Biol. Chem. 278*, 16389−16396.
15. Lusetti, S. L., Wood, E. A., Fleming, C. D., Modica, M. J., Korth, J., Abbott, L., Dwyer, D. W., Roca, A. I., Inman, R. B., and Cox, M. M. (2003) C-Terminal deletions of the *Escherichia coli* RecA protein. Characterization of *in vivo* and *in vitro* effects, *J. Biol. Chem. 278*, 16372−16380.
16. Lusetti, S. L., Shaw, J. J., and Cox, M. M. (2003) Magnesium ion-dependent activation of the RecA protein involves the C terminus, *J. Biol. Chem. 278*, 16381−16388.
17. Story, R. M., and Steitz, T. A. (1992) Structure of the recA protein-ADP complex, *Nature 355*, 374−376.
18. Story, R. M., Weber, I. T., and Steitz, T. A. (1992) The structure of the *E. coli* recA protein monomer and polymer, *Nature 355*, 318−325.
19. Xing, X., and Bell, C. E. (2004) Crystal structures of *Escherichia coli* RecA in a compressed helical filament, *J. Mol. Biol. 342*, 1471−1485.
20. Xing, X., and Bell, C. E. (2004) Crystal structures of *Escherichia coli* RecA in complex with MgADP and MnAMP-PNP, *Biochemistry 43*, 16142−16152.
21. Datta, S., Ganesh, N., Chandra, N. R., Muniyappa, K., and Vijayan, M. (2003) Structural studies on MtRecA-nucleotide complexes: Insights into DNA and nucleotide binding and the structural signature of NTP recognition, *Proteins: Struct., Funct., Genet. 50*, 474−485.
22. Datta, S., Krishna, R., Ganesh, N., Chandra, R. N., Muniyappa, K., and Vijayan, M. (2003) Crystal structures of *Mycobacterium smegmatis* RecA and its nucleotide complexes, *J. Bacteriol. 185*, 4280−4284.
23. Hortnagel, K., Voloshin, O. N., Kinal, H. H., Schaffer-Judge, N. M. C., and Camerini-Otero, R. D. (1999) Saturation mutagenesis of the *E. coli* RecA loop L2 homologous DNA pairing region reveals residues essential for recombination and recombinational repair, *J. Mol. Biol. 286*, 1097−1106.
24. Voloshin, O. N., Wang, L., and Camerini-Otero, R. D. (2000) The homologous pairing domain of RecA also mediates the allosteric regulation of DNA binding and ATP hydrolysis: A remarkable concentration of functional residues, *J. Mol. Biol. 303*, 709−720.
25. Stole, E., and Bryant, F. R. (1996) Reengineering the nucleotide cofactor specificity of the RecA protein by mutation of aspartic acid 100*, *J. Biol. Chem. 271*, 18326−18328.
26. Shan, Q., Cox, M. M., and Inman, R. B. (1996) DNA strand exchange promoted by RecA K72R, *J. Biol. Chem. 271*, 5712−5724.
27. Kelley, J. A., and Knight, K. L. (1997) Allosteric regulation of RecA protein function is mediated by Gln^{194}, *J. Biol. Chem. 272*, 25778−25782.
28. Brewer, S. H., Cresawn, S. G., Nguyen, D. T., and MacDonald, G. (2000) Difference FT-IR studies of nucleotide binding to the recombination protein RecA, *J. Phys. Chem. B 104*, 6950−6954.
29. Butler, B. C., Hanchett, R. H., Rafailov, H., and MacDonald, G. (2002) Investigating structural changes induced by nucleotide binding to RecA using difference FTIR, *Biophys. J. 82*, 2198−2210.
30. Barth, A., and Zscherp, C. (2002) What vibrations tell us about proteins, *Q. Rev. Biophys. 35*, 369−430.
31. Braiman, M. S., and Rothschild, K. J. (1988) Fourier transform infrared techniques for probing membrane protein structure, *Annu. Rev. Biophys. Biophys. Chem. 17*, 541−570.
32. Wojcik, E. J., Dalrymple, N. A., Alford, S. R., Walker, R. A., and Kim, S. (2004) Disparity in allosteric interactions of monastrol with Eg5 in the presence of ADP and ATP: A difference FT-IR investigation, *Biochemistry 43*, 9939−9949.
33. vonGermar, F., Galan, A., Llorca, O., Carrascosa, J. L., Valpuesta, J. M., Mantele, W., and Muga, A. (1999) Conformational changes generated in GroEL during ATP hydrolysis as seen by time-resolved infrared spectroscopy, *J. Biol. Chem. 274*, 5508−5513.

34. Jackson, M., and Mantsch, H. H. (1995) The use and misuse of FTIR spectroscopy in the determination of protein structure, *Crit. Rev. Biochem. Mol. Biol. 30*, 95−120.
35. Barth, A. (2000) The infrared absorption of amino acid side chains, *Prog. Biophys. Mol. Biol. 74*, 141−173.
36. Byler, D. M., and Susi, H. (1986) Examination of the secondary structure of proteins by deconvolved FTIR spectra, *Biopolymers 25*, 469−487.
37. El-Mahdaoui, L., and Tajmir-Riahi, H. A. (1995) A comparative study of ATP and GTP complexation with trivalent Al, Ga and Fe cations. Determination of cation binding site and nucleotide conformation by FTIR difference spectroscopy, *J. Biomol. Struct. Dyn. 13*, 69−86.
38. Cox, M. M., McEntee, K., and Lehman, I. R. (1981) A simple and rapid procedure for the large scale purification of the recA protein of *Escherichia coli*, *J. Biol. Chem. 256*, 4676−4678.
39. Bellamy, L. J. (1975) *The infrared spectra of complex molecules*, Vol. 1, Chapman and Hall, London.
40. Kim, S., and Barry, B. A. (1998) The protein environment surrounding tyrosyl radicals D and Z in photosystem II: A difference Fourier-transform infrared spectroscopic study, *Biophys. J. 74*, 2588−2600.
41. Venyaminov, S. Y., and Kalnin, N. N. (1990) Quantitative IR spectrophotometry of peptide compounds in water (H_2O) solutions. I. Spectral parameters of amino acid residue absorption bands, *Biopolymers 30*, 1243−1257.
42. Gerwert, K., Hess, B., and Englehard, M. (1990) Proline residues undergo structural changes during proton pumping in bacteriorhodopsin, *FEBS Lett. 261*, 449−454.
43. Takeuchi, H., Murata, H., and Harada, I. (1988) Interaction of adenosine 5′-triphosphate with Mg^{2+}: Vibrational study of coordination sties by use of ^{18}O-labeled triphosphates, *J. Am. Chem. Soc. 110*, 392−397.
44. Braiman, M. S., Briercheck, D. M., and Kriger, K. M. (1999) Modeling vibrational spectra of amino acid side chains in proteins: Effects of protonation state, counterion, and solvent on arginine C−N stretch frequencies, *J. Phys. Chem. B 103*, 4744−4750.
45. Hutson, M. S., Alexiev, U., Shilov, S. V., Wise, K. J., and Braiman, M. S. (2000) Evidence for a perturbation of arginine-82 in the bacteriorhodopsin photcycle from time-resolved infrared spectra, *Biochemistry 39*, 13189−13200.
46. Paulus, B. F., and Bryant, F. R. (1997) Time-dependent inhibition of RecA protein-catalyzed ATP hydrolysis by ATPγS: Evidence for a rate-determining isomerization of the RecA−ssDNA complex, *Biochemistry 36*, 7832−7838.
47. Ruigrok, R., and DiCapua, E. (1991) On the polymerization state of recA in the absence of DNA, *Biochimie 73*, 191−197.
48. Brenner, S. L., Zlotnick, A., and Griffith, J. D. (1988) RecA protein self-assembly. Multiple discrete aggregation states, *J. Mol. Biol. 204*, 959−972.
49. Pugh, B. F., and Cox, M. M. (1987) Stable binding of recA protein to duplex DNA: Unraveling a paradox, *J. Biol. Chem. 262*, 1326−1336.
50. Ye, J., Osborne, A. R., Groll, M., and Rapoport, T. A. (2004) RecA-like motor ATPases: Lessons from structures, *Biochim. Biophys. Acta 1659*, 1−18.
51. Konola, J. T., Nastri, H. G., Logan, K. M., and Knight, K. L. (1995) Mutations at Pro^{67} in the RecA protein P-loop motif differentially modify coprotease function and separate coprotease from recombination activites, *J. Biol. Chem. 270*, 8411−8419.
52. Konola, J. T., Guzzo, A., Gow, J.-B., Walker, G. C., and Knight, K. L. (1998) Differential cleavage of LexA and UmuD mediated by RecA Pro67 mutants: Implications for common LexA and UmuD binding sites on RecA, *J. Mol. Biol. 276*, 405−415.
53. Eldin, S., Forget, A. L., Lindenmuth, D. M., Logan, K. M., and Knight, K. L. (2000) Mutations in the N-terminal region of RecA that disrupt the stability of free protein oligomers but not RecA-DNA complexes, *J. Mol. Biol. 299*, 91−101.
54. Logan, K. M., Forget, A. L., Verderese, J. P., and Knight, K. L. (2001) ATP-mediated changes in cross-subunit interactions in the RecA protein, *Biochemistry 40*, 11382−11389.
55. Yamazaki, J., Horii, T., Sekiguchi, M., and Takahashi, M. (2003) Regulation of RecA protein binding to DNA by opposing effects of ATP and ADP on inter-domain contacts: Analysis by urea-induced unfolding of wild-type and C-terminal truncated RecA, *J. Mol. Biol. 329*, 363−370.
56. Ramreddy, T., Sen, S., Rao, B. J., and Krishnamoorthy, G. (2003) DNA dynamics in RecA-DNA filaments: ATP hydrolysis-related flexibility in DNA, *Biochemistry 42*, 12085−12094.

BI047362U